Technical Note: Experimental verification of magnetic field-induced beam deflection and Bragg peak displacement for MR-integrated proton therapy

Sonja M. Schellhammer and Sebastian Gantz
OncoRay – National Center for Radiation Research in Oncology, Faculty of Medicine and University Hospital Carl Gustav Carus, Technische Universität Dresden, Helmholtz-Zentrum Dresden – Rossendorf, Dresden 01307, Germany
Institute of Radiooncology – OncoRay, Helmholtz-Zentrum Dresden – Rossendorf, Dresden 01328, Germany

Armin Lühr
OncoRay – National Center for Radiation Research in Oncology, Faculty of Medicine and University Hospital Carl Gustav Carus, Technische Universität Dresden, Helmholtz-Zentrum Dresden – Rossendorf, Dresden 01307, Germany
Institute of Radiooncology – OncoRay, Helmholtz-Zentrum Dresden – Rossendorf, Dresden 01328, Germany
German Cancer Consortium (DKTK), Partner Site Dresden, and German Cancer Research Center (DKFZ), Heidelberg 69120, Germany

Bradley M. Oborn
Centre for Medical Radiation Physics, University of Wollongong, Wollongong 2522, Australia
Illawarra Cancer Care Centre, Wollongong Hospital, Wollongong 2522, Australia

Michael Bussmann
Institute of Radiation Physics, Helmholtz-Zentrum Dresden – Rossendorf, Dresden 01328, Germany

Aswin L. Hoffmann[a]
OncoRay – National Center for Radiation Research in Oncology, Faculty of Medicine and University Hospital Carl Gustav Carus, Technische Universität Dresden, Helmholtz-Zentrum Dresden – Rossendorf, Dresden 01307, Germany
Institute of Radiooncology – OncoRay, Helmholtz-Zentrum Dresden – Rossendorf, Dresden 01328, Germany
Department of Radiotherapy and Radiation Oncology, Faculty of Medicine and University Hospital Carl Gustav Carus, Technische Universität Dresden, Dresden 01307, Germany

Purpose: Given its sensitivity to anatomical variations, proton therapy is expected to benefit greatly from integration with magnetic resonance imaging for online anatomy monitoring during irradiation. Such an integration raises several challenges, as both systems mutually interact. The proton beam will experience quasi-continuous energy loss and energy-dependent electromagnetic deflection at the same time, giving rise to a deflected beam trajectory and an altered dose distribution with a displaced Bragg peak. So far, these effects have only been predicted using Monte Carlo and analytical models, but no clear consensus has been reached and experimental benchmark data are lacking. We measured proton beam trajectories and Bragg peak displacement in a homogeneous phantom placed inside a magnetic field and compared them to simulations.
Methods: Planar dose distributions of proton pencil beams (80–180 MeV) traversing the field of a 0.95 T NdFeB permanent magnet while depositing energy in a PMMA slab phantom were measured using EBT3 radiochromic films and simulated using the Geant4 toolkit. Deflected beam trajectories and the Bragg peak displacement were extracted from the measured planar dose distributions and compared against the simulations.
Results: The lateral beam deflection was clearly visible on the EBT3 films and ranged from 1 to 10 mm for 80 to 180 MeV, respectively. Simulated and measured beam trajectories and Bragg peak displacement agreed within 0.8 mm for all studied proton energies.
Conclusions: These results prove that the magnetic field-induced Bragg peak displacement is both measurable and accurately predictable in a homogeneous phantom at 0.95 T, and allows Monte Carlo simulations to be used as gold standard for proton beam trajectory prediction in similar frameworks for MR-integrated proton therapy. © *2018 American Association of Physicists in Medicine* [https://doi.org/10.1002/mp.12961]

1. INTRODUCTION

The main rationale for the increasing interest in proton therapy in the field of radiation oncology has been its favorable dose profile which features a steep maximum, the so-called Bragg peak.[1] This peak allows for applying a high-dose gradient at the distal end of the target volume, thereby sparing healthy tissue behind the tumor. At the same time, the

steepness of the Bragg peak and its positional dependence on the material composition in the beam path make proton treatment far more sensitive to morphological changes in the patient than photon therapy. Anatomical changes and differences in patient positioning between irradiations (interfractional uncertainties) as well as during irradiation (intrafractional uncertainties) lead to considerable uncertainties in the dose delivery.[2] These uncertainties currently translate into large treatment margins around the tumor and thus compromise the dosimetric benefit of proton therapy, which can lead to undesired treatment toxicity. Although pretreatment image guidance (e.g., in-room or on-board cone-beam computed tomography) is becoming more readily accessible, it cannot fully account for intrafractional motion and deformation, which can be significant for moving tumours of the thorax and abdomen region.[3]

One strategy to reduce this treatment toxicity is to monitor the patient's anatomy during dose delivery in real time and to adapt the beam accordingly. Providing unmatched soft-tissue contrast, subsecond temporal resolution, and the absence of ionizing radiation dose, magnetic resonance imaging (MRI) appears to be an ideal candidate for anatomy monitoring during treatment delivery.[4] For photon beam therapy, the integration of both modalities has already been realized,[5,6] and the first-generation hybrid systems have recently found their way into clinical application.[7,8]

Because of the high-anatomical sensitivity of proton therapy, the integration of MRI into proton therapy (MRiPT) is expected to be even more beneficial than for photon therapy and thus has gained interest in the last years.[9,10] However, MRiPT has only been studied on a conceptual level thus far, as a number of technical and physical challenges need to be overcome. Mutual interactions are expected between the electromagnetic fields of the MR scanner and the proton beam line.[10,11] Furthermore, unlike photons, protons being charged particles are subject to the Lorentz force when traversing the magnetic field of an MRI scanner, causing the beam to be deflected from its otherwise straight path.

As this deflection is energy dependent, the quasi-continuous energy loss of protons interacting with substances of the human body will affect the local curvature of the beam as it penetrates the body. A number of simulation studies have been performed using Monte Carlo methods or (semi-)analytical approaches to investigate deflected beam trajectories of monoenergetic beams in a water phantom or patient placed in a uniform magnetic field, and considerable distortions of the dose distribution in the patient have been predicted. Particularly, the Bragg peak is expected to be displaced by a few millimeters up to several centimeters, depending on the beam energy and magnetic flux density distribution.[12,13,14,15,16,17]

However, there is no clear consensus on the exact amount of magnetic field-induced Bragg peak displacement to be expected in tissue-like materials,[17] and experimental benchmark data do not exist. We, therefore, perform a first measurement thereof and compare it against Monte Carlo-based predictions.

2. MATERIALS AND METHODS

The measurement setup is depicted in Fig. 1. It consists of a collimated proton beam, a slab phantom containing a horizontally placed film dosimeter, and a permanent magnet assembly.

The proton beam was generated by an isochronous cyclotron (C230, IBA, Louvain-La-Neuve, Belgium) at University Proton Therapy Dresden (UPTD). The horizontal static beam line was used and defined the x-axis of the setup. The beam was collimated to a cylindrical pencil beam of 10 mm diameter in order to prevent the magnet from being damaged by direct radiation exposure. The collimated beam diameter at the phantom entrance was smaller than 1.5 cm (full width tenth maximum) thus sparing the magnet assembly.

The slab phantom was produced from polymethyl methacrylate (PMMA) and mounted horizontally in the 4 cm wide air gap between the poles of a C-shaped permanent magnet assembly. It consisted of two slabs, such that a film dosimeter was placed horizontally in the central plane parallel to the beam, allowing to measure the full-deflected beam trajectory. The contact area of the slabs was bevelled by $\alpha = 1°$ around the y-axis to reduce the dependence of the dose distribution on the film material and on possible air gaps between the phantom and the film.[18] Two vertically oriented pins in the phantom and corresponding holes in the films ensured a reproducible alignment of the film relative to the phantom.

A self-developing Gafchromic EBT3 film detector of 280 μm thickness (Ashland, Covington, USA) was used to measure the planar dose distributions in the central plane of the proton beam. This dosimeter type was chosen over alternatives such as ionization chambers, scintillators, thermoluminescent (TLD), optically stimulated luminescent (OSL), and gel dosimeters because it provides a continuous two-dimensional measurement with submillimeter spatial resolution that is largely unaffected by magnetic fields,[19] well-established, easy to handle and readily available.

The phantom incorporating the film detector was placed inside a transversal magnetic field (see Appendix, Fig. B.4 in Supporting Information) produced by a magnet assembly comprising two $Nd_2Fe_{14}B$ permanent magnet poles and a yoke. The maximum magnetic flux density of $B_0 = 0.95$ T was comparable to that of existing MR-integrated photon therapy systems with flux densities between 0.35 T and 1.5 T.[5,6,7,20] The main field component defined the z-axis of the setup (pointing downward) and caused a deflection of the proton beam in the (positive) y-direction. In order to measure the whole trajectory of the protons slowing down inside the main magnetic field, the beam energy was limited to 180 MeV. The experiment was performed with and without the magnet present.

Two-dimensional dose distributions $D(x,y)$ were obtained on the film plane. From these, the beam trajectory and Bragg peak displacement were extracted as follows. For each depth x, a univariate Gaussian function was fitted to the lateral beam profile and the maximum position $y_T(x)$ was extracted.
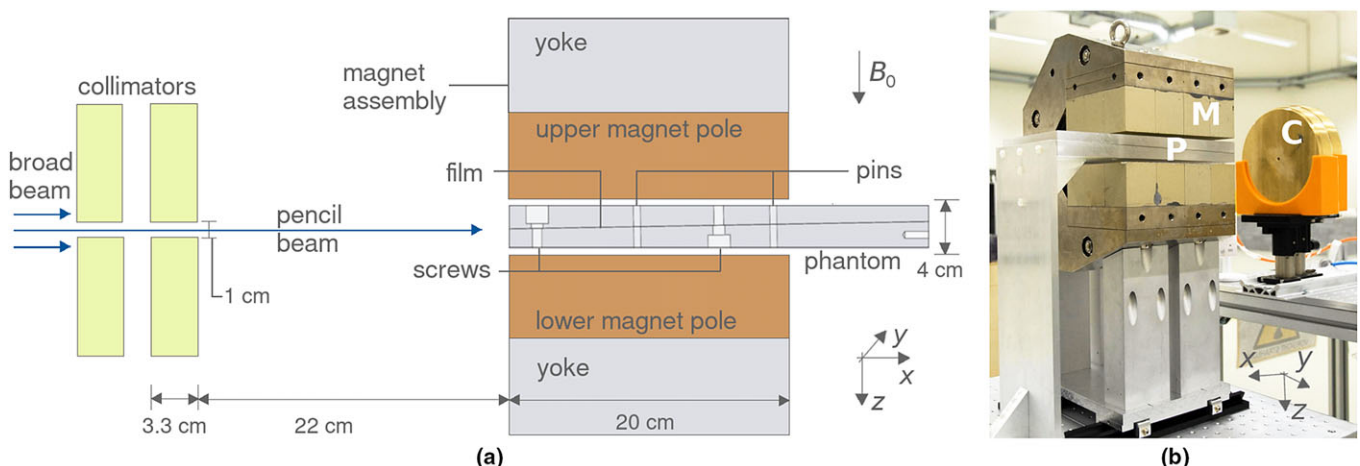
FIG. 1. Schematic sagittal view (a) and photograph (b) of the experimental setup. The proton beam passed through collimators (C) and a slab phantom (P) placed inside the field of a permanent magnet (M). The dose in the phantom was measured using a Gafchromic film detector. A left-handed coordinate system is used. Photo edited for clarity. [Color figure can be viewed at wileyonlinelibrary.com]

This yielded the beam trajectory $y_T(x)$. To mimic a depth–dose curve measured by an ionization chamber of 8 cm diameter, for each depth, the predicted dose was integrated radially around $y_T(x)$ with an integration radius of $r = 4$ cm. This resulted in the integral depth–dose curve,

$$IDD(x) = \int_0^{2\pi} \int_0^r D(x, \rho, \phi) \rho \, d\rho \, d\phi$$
$$= \pi \int_{-r}^r D(x, y)|y - y_T(x)| \, dy, \qquad (1)$$

where ρ and ϕ are the polar coordinates. Both $y_T(x)$ and $IDD(x)$ were smoothed to reduce statistical noise using a univariate spline fit. The mean of the first proximal ten values of $y_T(x)$ was subtracted from $y_T(x)$ to achieve $y_T(0) \approx 0$. The range R_{80} was calculated from $IDD(x)$ as the depth of the beam at the 80% distal end of the IDD maximum. The longitudinal Bragg peak retraction was defined as the difference between R_{80} with and without magnetic field. The lateral Bragg peak deflection was determined from the beam trajectory obtained with magnetic field as $y_T(R_{80})$.

The measured data allowed for a verification of Monte Carlo-based particle tracking simulations, being considered as the gold standard for dose calculation in radiation therapy planning. The measurement setup was simulated using the Geant4 toolkit version 10.2.p02[21,22] and beam trajectories

and Bragg peak displacement were extracted as stated above. The magnetic field map for the simulation was generated using finite-element modelling (COMSOL Multiphysics, COMSOL AB, Stockholm, Sweden). This map was validated in all three magnetic field components by measurements in the central horizontal plane and in one quadrant of the air gap between the magnet poles at 5 mm resolution using an automated magnetometry setup comprising a robotic-positioning device and a Hall probe (MMTB-6J04-VG, Lake Shore Cryotronics, Westerville, USA) connected to a Gaussmeter (Model 421, Lake Shore Cryotronics). The beam model was validated by depth–dose and profile measurements in water and air without magnetic field (see Appendix B.2 in Supporting Information).

Details on the experimental methods and Monte Carlo simulations are given in Appendices A and B, respectively.

3. RESULTS

3.A. Measured beam deflection and Bragg peak dislocation

The influence of the magnetic field on the proton dose distribution could be observed on the film dosimeter signal, as depicted in Fig. 2. The characteristic shape of the proton dose
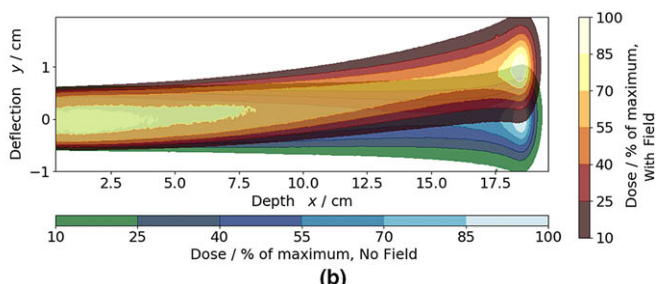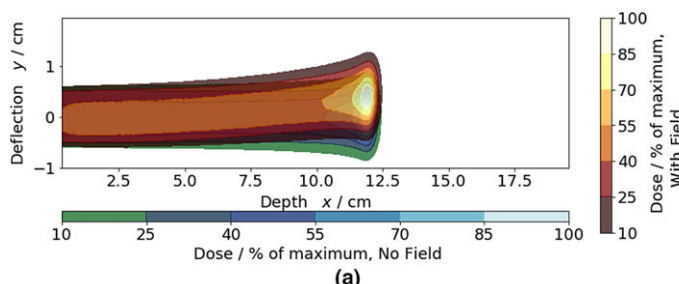

FIG. 2. Relative dose distribution of a 140 MeV (a) and a 180 MeV (b) proton beam in PMMA measured with the film dosimeter, without (bluescale, bottom) and with (redscale, top) magnetic field. [Color figure can be viewed at wileyonlinelibrary.com]
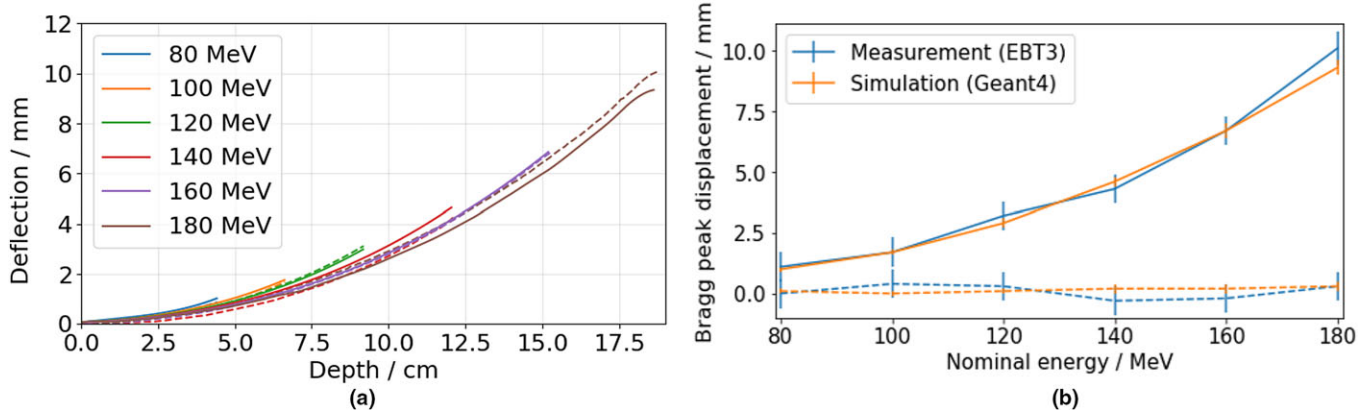
FIG. 3.   (a) Monte Carlo calculated (solid lines) and measured (dashed) deflected central beam trajectories. (b) Calculated and measured magnetic field-induced Bragg peak displacement in lateral (deflection, solid) and longitudinal (retraction, dashed) direction. Error bars refer to systematic and statistical uncertainties given in Tables A.1 and B.4 in Supporting information. Individual data points are interconnected for visualization only. [Color figure can be viewed at wileyonlinelibrary.com]

distribution was visible both with and without magnetic field. However, with magnetic field, the beam followed a deflected trajectory resulting in a laterally shifted Bragg peak position.

The measured lateral deflection of the Bragg peak ranged from 1 mm for 80 MeV up to 10 mm for 180 MeV. Bragg peak retraction was within measurement uncertainty and ≤0.5 mm for all studied energies. As expected, the deflected beam trajectories [see Fig. 3(a)] did not coincide for different energies, but fanned out energy dependently, as the radius of beam path increases with increasing proton energy.[13,17] No magnetic field-induced change in the absolute measured dose was observed.

3.B. Comparison of simulation and experiment

The predicted and measured deflected central beam trajectories agreed within 0.8 mm for all studied beam energies [see Fig. 3(a)]. To quantify the accuracy of the calculated Bragg peak positions, their retraction and deflection were compared [see Fig. 3(b)]. The uncertainties of the measured and simulated Bragg peak displacement were within 0.5 and 0.3 mm, respectively (see Appendix A.3 and Appendix B.5 in Supporting Information). Predicted and measured Bragg peak retraction and deflection agreed within these uncertainties for all studied energies. There was no systematic difference in both quantities between the simulation and measurement data.

4. DISCUSSION

The obtained range in Bragg peak displacement of 1–10 mm corresponds well with previous theoretical studies in a homogeneous magnetic field in water.[16,17] As opposed to a previous study for photons,[23] no systematic differences in absolute dose were found between the film measurements with and without magnetic field, which may be caused by the fact that film dosimeters were oriented perpendicular to the magnetic field in this study.

Due to the LET-dependent dose saturation of EBT3 films, no direct dose comparison was made between measurements and Monte Carlo simulations. While this study aimed to quantify the accuracy of the predicted beam deflection and Bragg peak displacement (which was found to be affected by this saturation by 0.2 mm or less), commissioning procedures of future MRiPT systems will need to include extensive three-dimensional dose measurements corrected for such effects.

This study has been confined to a homogeneous medium. For inhomogeneous media, a magnetic field-induced dose enhancement at medium-air material boundaries in the order of 2% has been predicted for 250 MeV and 3 T caused by electrons returning to the material boundary after being deflected by Lorentz force in air.[16] For media other than PMMA, changes in stopping power affect the range and the local beam curvature, and thus, the displacement of the Bragg peak.[17] Therefore, future measurements in inhomogeneous media are desirable. However, the conclusions drawn in this study are expected to be transferable to other tissue-like media, as the underlying particle interactions do not differ substantially.

5. CONCLUSION

Magnetic field-induced deflection of a slowing-down therapeutic proton beam in a tissue-like medium has been measured by film dosimetry and compared against particle-tracking simulations. In a transverse magnetic field of 0.95 T, it was shown that the lateral Bragg peak displacement ranges between 1 and 10 mm for proton energies between 80 and 180 MeV in PMMA. Range retraction was found to be ≤0.5 mm. The measured Bragg peak displacement was shown to agree within 0.8 mm with Monte Carlo-based particle tracking simulations.

This work has shown for the first time that the magnetic field-induced proton beam deflection and Bragg peak displacement are both measurable and accurately predictable in

a tissue-like beam stopping medium. Within the given uncertainties and over the studied range of proton energy and magnetic flux density, the presented verification of Monte Carlo-based trajectory prediction allows future Monte Carlo studies to bring a consensus which of the different analytical and numerical models for Bragg peak displacement prediction is the most accurate one and should hence be used in future treatment planning systems for MR-integrated proton therapy.

ACKNOWLEDGMENTS

CONFLICTS OF INTEREST

The authors have no conflicts to disclose.

[a] Author to whom correspondence should be addressed. Electronic mail: aswin.hoffmann@hzdr.de.

REFERENCES

1. Jäkel O. Medical physics aspects of particle therapy, *Radiat Prot Dosimetry.* 2009;137:56–166.
2. de Ruysscher D, Sterpin E, Haustermans K, Depuydt T. Tumour movement in proton therapy: solutions and remaining questions: a review. *Cancers.* 2015;7:1143–1153.
3. Engelsman M, Bert C. Precision and uncertainties in proton therapy for moving targets. In: Paganetti H, ed. *Proton Therapy Physics*. Boca Raton, FL: CRC Press, Taylor & Francis Group; 2011.
4. Lagendijk JJW, Raaymakers BW, van den Berg CAT, Moerland MA, Philippens ME, van Vulpen M. MR guidance in radiotherapy. *Phys Med Biol.* 2014;59:R349–R369.
5. Fallone BG. The rotating biplanar linac-magnetic resonance imaging system. *Semin Radiat Oncol.* 2014;24:200–202.
6. Keall PJ, Barton M, Crozier S. The Australian magnetic resonance imaging-linac program. *Semin Radiat Oncol.* 2014;24:203–206.
7. Mutic S, Dempsey J. The ViewRay system: magnetic resonance-guided and controlled radiotherapy. *Semin Radiat Oncol.* 2014;24:196–199.
8. Raaymakers BW, Jürgenliemk-Schulz IM, Bol GH, et al. First patients treated with a 1.5 T MRI-Linac: clinical proof of concept of a high-precision, high-field MRI guided radiotherapy treatment. *Phys Med Biol.* 2017;62:L41–L50.
9. Oborn BM, Dowdell S, Metcalfe PE, Crozier S, Mohan R, Keall PJ. Future of medical physics: real-time MRI guided proton therapy. *Med Phys.* 2017;44:e77–e90.
10. Oborn BM, Dowdell S, Metcalfe PE, Crozier S, Mohan R, Keall PJ. Proton beam deflection in MRI fields: implications for MRI-guided proton therapy. *Med Phys.* 2015;42:2113–2124.
11. Oborn BM, Dowdell S, Metcalfe PE, et al. MRI Guided Proton Therapy: Pencil beam scanning in an MRI fringe field, ICTR-PHE, Geneva, February 15-19 02 2016.
12. Raaymakers B, Raaijmakers AJE., Lagendijk JJ. Feasibility of MRI guided proton therapy: magnetic field dose effects. *Phys Med Biol.* 2008;53:5615–5622.
13. Wolf R, Bortfeld T. An analytical solution to proton Bragg peak deflection in a magnetic field. *Phys Med Biol.* 2012;57:N329–N337.
14. Moteabbed M, Schuemann J, Paganetti H. Dosimetric feasibility of real-time MRI-guided proton therapy. *Med Phys.* 2014;41:1–11.
15. Hartman J, Kontaxis C, Bol GH, Frank SJ, et al. Dosimetric feasibility of intensity modulated proton therapy in a transverse magnetic field of 1.5 T. *Phys Med Biol.* 2015;60:5955–5969.
16. Fuchs H, Moser P, Gröschl M, Georg D. Magnetic field effects on particle beams and their implications for dose calculation in MR guided particle therapy. *Med Phys.* 2017;44:1149–1156.
17. Schellhammer SM, Hoffmann AL. Prediction and compensation of magnetic beam deflection in MR-integrated proton therapy: a method optimized regarding accuracy, versatility and speed. *Phys Med Biol.* 2017;62:1548–1564.
18. Zhao L, Das IJ. Gafchromic EBT Film dosimetry in proton beams. *Phys Med Biol.* 2010;55:N291–N301.
19. Wang J, Rubinstein A, Ohrt J, Ibbott G, Wen Z. Effect of a strong magnetic field on TLDs, OSLDs, and Gafchromic films using an electromagnet. *Med Phys.* 2016;43:3873–3874.
20. Lagendijk JJ, Raaymakers BW, van Vulpen M. The magnetic resonance imaging-linac system. *Semin Radiat Oncol.* 2014;24:207–209.
21. Agostinelli S, et al. Geant4 - a simulation toolkit. *Nucl Instrum Meth Phys Res Sect A.* 2003;506:250–303.
22. Allison J, et al. Geant4 developments and applications. *IEEE Trans Nucl Sci* 2006;53:270–278.
23. Delfs B, Schoenfeld AA, Poppinga D, et al. Magnetic fields are causing small, but significant changes of the radiochromic EBT3 film response to 6 MV photons. *Phys Med Biol.* 2018;63:035028.
24. Vacuumschmelze. Selten-Erd-Dauermagnete Vacodym Vacomax, Grüner Weg 37, 63450 Hanau/Germany; 2014.
25. Zeil K, Beyreuther E, Lessmann E, Wagner W, Pawelke J. Cell irradiation setup and dosimetry for radiobiological studies at ELBE. *Nucl Instrum Meth Phys Res B* 2009;26:2403–2410.
26. Sorriaux J, Kacperek A, Rossomme S, et al. Evaluation of Gafchromic EBT3 films characteristics in therapy photon, electron and proton beams. *Phys Med.* 2012;29:599–606.
27. Wohlfahrt P, Möhler C, Richter C, Greilich S. Evaluation of stopping-power prediction by dual- and single-energy computed tomography in an anthropomorphic ground-truth phantom. *IJROBP.* 2018;100:244–253.
28. Bortfeld T. An analytical approximation of the Bragg curve for therapeutic proton beams. *Med Phys.* 1997;24:2024–2033.
29. Berger MJ, Coursey JS, Zucker MA, Chang J. ESTAR, PSTAR, and ASTAR: Computer Programs for Calculating Stopping-Power and Range Tables for Electrons, Protons, and Helium Ions, National Institute of Standards and Technology, Gaithersburg, MD, Version 1.2.3, Retrieved Apr 27, 2015; 2005.
30. Almhagen E. Development and validation of a scanned proton beam model for dose distribution verification using Monte Carlo, Master's thesis, Stockholm University; 2015.
31. Geant4 collaboration. Reference Physics Lists, retrieved Aug 18, 2016; 2013. URL http://geant4.cern.ch/support/proc_mod_catalog/physics_lists/referencePL.shtml
32. Geant4 collaboration. Geant4 10.1 Release Notes, retrieved Aug 18, 2016; 2014. URL http://geant4.cern.ch/support/ReleaseNotes4.10.1.html
33. Perl J, et al. TOPAS documentation: Default Parameters, retrieved Dec 27, 2017; 2016. URL http://topas.readthedocs.io/en/latest/parameters/defaults.html
34. Grevillot L, Frisson T, Zahra N, et al. Optimization of GEANT4 settings for proton pencil beam scanning simulations using GATE. *Nucl Instrum Meth Phys Res Sect B.* 2010;268:3295–3305.
35. GATE collaboration. Documentation and Recommendations for Users, retrieved Aug 18, 2016; 2017. URL http://www.opengatecollaboration.org/UsersGuide
36. ICRU. Stopping of ions heavier than Helium, ICRU Report 73.
37. James F. A review of pseudorandom number generators. *Comput Phys Commun.* 1990;60:329–344.
38. Schellhammer SM, Matthes A, Pipek J, Apostolakis J. Problem 1879 - Segfault at magnetic field edges, retrieved Nov 15, 2016; 2017. URL https://bugzilla-geant4.kek.jp/show_bug.cgi?id=1879
39. Kurosu K, Takashina M, Koizumi M, Das IJ, Moskvin V. Optimization of GATE and PHITS Monte Carlo code parameters for uniform scanning proton beam based on simulation with FLUKA general-purpose code. *Nucl Instrum Meth Phys Res Sect B* 2014;336:45–54.

40. Arjomandy B, Tailor R, Zhao L, Devic S. EBT2 film as a depth-dose measurement tool for radiotherapy beams over a wide range of energies and modalities. *Med Phys.* 2012;39:912–921.

41. Perles LA, Mirkovic D, Anad A, Titt U, Mohan R. LET dependence of the response of EBT2 films in proton dosimetry modeled as a bimolecular chemical reaction. *Phys Med Biol.* 2013;58:8477–8491.

42. Gantz S. Characterization of the magnetic field of a 0.95 T permanent dipole magnet and experimental validation of proton beam deflection in a magnetic field within tissue-equivalent material, Master's thesis, TU Dresden; 2017.

SUPPORTING INFORMATION

Additional Supporting Information may be found online in the supporting information section at the end of the article.

Appendix A. Experimental measurements
Appendix B. Monte Carlo simulations